An Analysis of the Linkage of Pacific Subtropical Cells with the Recharge–Discharge Processes in ENSO Evolution

HAN-CHING CHEN AND CHUNG-HSIUNG SUI

Department of Atmospheric Sciences, National Taiwan University, Taipei, Taiwan

YU-HENG TSENG

Ocean Section, Climate and Global Dynamics Division, National Center for Atmospheric Research, Boulder, Colorado

BOHUA HUANG

Department of Atmospheric, Oceanic, and Earth Sciences, College of Science, George Mason University, Fairfax, Virginia

(Manuscript received 17 February 2014, in final form 8 February 2015)

ABSTRACT

The Simple Ocean Data Assimilation, version 2.2.4 (SODA 2.2.4), analysis for the period of 1960–2010 is used to study the variability of Pacific subtropical cells (STCs) and its causal relation with tropical climate variability. Results show that the interior STC transport into the equatorial basin through 9°S and 9°N is well connected with equatorial sea surface temperature (SST) (9°S–9°N, 180°–90°W). The highest correlation at interannual time scales is contributed by the western interior STC transport within 160°E and 130°W. It is known that the ENSO recharge–discharge cycle experiences five stages: the recharging stage, recharged stage, warmest SST stage, discharging stage, and discharged stage. A correlation analysis of interior STC transport convergence, equatorial warm water volume (WWV), wind stress curl, and SST identifies the time intervals between the five stages, which are 8, 10, 2, and 8 months, respectively. A composite analysis for El Niño–developing and La Niña–developing events is also performed. The composited ENSO evolutions are in accordance with the recharge–discharge theory and the corresponding time lags between the above denoted five stages are 4–12, 6, 2, and 4 months, respectively. For stronger El Niño events, the discharge due to interior STC transport at 9°N terminates earlier than that at 9°S because of the southward migration of westerly winds following the El Niño peak phase. This study clarifies subsurface transport processes and their time intervals, which are useful for refinement of theoretical models and for evaluating coupled ocean–atmosphere general circulation model results.

1. Introduction

Several early works (Wyrtki 1975; White et al. 1985) emphasized the importance of ocean dynamics and suggested that a buildup of warm water in the western equatorial Pacific was a necessary precondition to the development of El Niño. Wyrtki (1985) calculated the warm water volume (WWV) variability between 15°S and 15°N by integrating sea level variability. He showed that the WWV of the tropical Pacific tends to increase as a whole prior to an El Niño event, and then decreases during the course of the event. Jin (1997a,b) proposed a theoretical ''recharge–discharge oscillator'' paradigm to describe how the WWV could control the timing of El Niño and La Niña events. Meinen and McPhaden (2000, 2001) used in situ measurements of subsurface temperature to demonstrate Jin's hypothesized oscillator. These studies show that the recharge and discharge processes can be estimated by variations of the WWV, defined as the volume of water warmer than 20°C representing the upper-ocean heat content. Prior to the mature phase of El Niño events by 6–7 months (Jin 1997a; Meinen and McPhaden 2000, 2001), the WWV builds up in the tropics, increasing the mean thermocline depth along the equator and preconditioning the ocean to swing into the warm phase. During the mature warm phase, the warm water is transported to the

Corresponding author address: Dr. Chung-Hsiung Sui, Department of Atmospheric Sciences, National Taiwan University, No. 1, Sec. 4, Roosevelt Rd., Taipei 10617, Taiwan.
E-mail: sui@as.ntu.edu.tw

DOI: 10.1175/JCLI-D-14-00134.1

off-equatorial Pacific, which reduces the mean thermocline depth along the equator and sets up a condition for a La Niña event to occur.

The subtropical cells (STCs), also known as shallow meridional overturning circulations, provide an oceanic mechanism connecting the extratropics and tropics. The STCs are mainly driven by surface wind forcing (McCreary and Lu 1994; Lu et al. 1998) and consist of subtropical water mass that subducts in the eastern ocean, flows westward and equatorward in the upper pycnocline layers through both western boundary and interior pathway (interior STCs), feeds into the equatorial undercurrent, and upwells into surface equatorial water before returning to the subtropics in the surface Ekman layer (McCreary and Lu 1994; Rothstein et al. 1998). The STCs play an important role in redistributing mass, heat, and salt between the extratropical and equatorial oceans. Previous studies have found that the strength of the interior STCs is largely anticorrelated with equatorial sea surface temperature (SST) changes at both interannual and decadal time scales (Capotondi et al. 2005). The interannual variability of STCs and the recharge–discharge oscillator appear related, but as far as we know, the causal relation between the subtropical and tropical process has not been studied in detail.

One major limitation in studying the linkage of STCs with El Niño events is the lack of direct observations to measure the strength and transport of STCs accurately. Current estimates based on available historical hydrographic observations may have large uncertainties because of the sparseness of the historical measurements in both time and space. On the other hand, numerical simulations of the ocean general circulation models (OGCMs), which calculate ocean currents directly, may suffer from systematic bias, such as the diffused thermocline, to reproduce the STC path, strength, and water properties realistically. Therefore, ocean reanalysis datasets, which combine oceanic observations and OGCMs through data assimilation, may be a promising alternative approach to better represent the STCs.

Another limiting factor in the study of STC transport is that the meridional mass transport, as well as its variability, is not uniformly distributed in the Pacific basin. Several studies discussed the relation of the meridional transport variability between the western boundary and interior STCs. Both realistic and idealized model simulations have shown a large compensation between the variability of STC transport and western boundary transport (Springer et al. 1990; Lee and Fukumori 2003; Hazeleger et al. 2004; Wang et al. 2003; Ishida et al. 2008). Previous studies also revealed some complex structures in the interior STC transport (Kumar and Hu 2014; Bosc and Delcroix 2008). These spatial variations may affect the efficiency of the recharge–discharge process. In fact, the compensating effect between the eastern and western STCs, as well as those associated with the western boundary current and the asymmetry between the southern and northern cells (to be discussed later in this study), can affect the net meridional mass convergence. As a result, the speed of recharge/discharge of mass may be slower compared to what we expect from the traditional theory. As the recharge/discharge of mass becomes slower (or quicker), the period of ENSO is longer (shorter). The detailed structure of the meridional cell can be one of the factors that determine the properties of ENSO.

To alleviate the above limitations, we investigate the variations of Pacific STC transport and its relationship with equatorial SST in the Simple Ocean Data Assimilation (SODA) reanalysis, version 2.2.4, from 1960 to 2010. Our study has three specific purposes. First, we intend to examine the mutual consistency on the STC variability between the observation of McPhaden and Zhang (2002, hereafter MPZ) and the SODA data. On one hand, the estimation of STCs in MPZ is based on the available sparse hydrographic measurements so that the variations in western boundary current transport cannot be reliably estimated. On the other hand, the SODA data are based on observations, physics, and an advanced assimilation method that can provide all ocean fields at higher resolution. However, since SODA is an assimilation product and heat and salt are not totally conserved, the WWV may change even without any meridional transport associated with the STCs. This is consistent with our analysis that the mass budget is not perfectly closed for a volume above a surface of constant potential density within the tropical Pacific basin. On the other hand, our results show that the qualitative relationship between the WWV changes and the volume convergence still holds reasonably well. Therefore, even though such an inadequacy prevents us from doing a quantitative analysis of the mass budget for the recharge–discharge process, we can still use the data to qualitatively understand the physical mechanism of the recharge–discharge process. Second, we analyze the spatial structure of interior STC transport convergence variability to take into account the different response of the eastern and western interior STC transport to the equatorial SST anomaly on interannual time scales. For El Niño events, the surface westerly wind anomalies dominate over the central Pacific and only weak anomalous easterly winds are found in the far eastern Pacific. These winds with opposite directions in the eastern and central Pacific force different regional responses in the interior STC transport. Finally, we seek a better understanding of ENSO evolution involving interior STC

transport in the context of the recharge–discharge oscillator theory. In our study, we investigate the relationship between equatorial SST, interior STC transport, and WWV in recharge–discharge oscillator theory and time intervals of the ENSO cycle.

In this study, section 2 introduces the SODA data. In section 3, we show the STC variability and the time series of interior STC transport and equatorial SST. Section 4 examines the relationship between interior STC convergence and equatorial SST at various longitudes. Based on recharge–discharge theory, we further study the connection between interior STC transport and SST using correlation analysis in section 5 and using composite analysis in section 6. In section 7, we study the meridional asymmetry of meridional mass transport. The summary and a discussion are given in section 8.

2. Data

The ocean temperature, current, salinity, and wind stress variables are taken from the SODA reanalysis version 2.2.4 (Giese and Ray 2011). SODA 2.2.4 is derived from the ocean data assimilation procedure using a general circulation model based on Parallel Ocean Program (POP) physics with an average 0.25° × 0.4° horizontal and 40-level vertical resolution. Observations assimilated into the ocean model include all available hydrographic profile data, ocean station data, moored temperature and salinity measurements, in situ temperature and salinity observations from instrument of various types [e.g., mechanical bathythermograph (MBT), XBT, and CTD], and SST from nighttime infrared measurement. However, current velocity data are not assimilated in the SODA product because very few such observations are available. The monthly output is mapped onto a uniform global 0.5° × 0.5° horizontal grid with 40 levels in the vertical. The surface boundary conditions are obtained from the ensemble members from atmospheric reanalysis Twentieth-Century Reanalysis, version 2 (20CRv2) (Whitaker at al. 2004; Compo et al. 2006, 2011). More information can be found in Carton et al. (2005) and Carton and Giese (2008). Although the data are available from 1871 to 2010, here we analyze the output from 1960 to 2010 when the observations are relatively abundant and the reanalysis is more reliable. The SST in SODA 2.2.4 (taken at 5-m depth) from 1960 to 2010 is highly consistent with Met Office Hadley Centre Sea Ice and Sea Surface Temperature dataset, version 1 (HadISST1; Rayner et al. 2003). In this study, we used a 2–8-yr bandpass filter to isolate interannual variability (interannual time scales).

3. STC variability

Following MPZ, we calculate the meridional transport across 9°S and 9°N. The latitude of 9°N is chosen because it represents a choke point for the meridional geostrophic transport between the extratropics and tropics owing to the existence of a potential vorticity ridge at 9°N (MPZ), and 9°S is chosen for hemispheric symmetry. Longitude–depth sections of time-mean meridional velocities across 9°S and 9°N are shown in Fig. 1. Across both latitudes, the poleward surface Ekman transport of STCs is confined approximately to the upper 50 m, and the pycnocline transport of STCs is found primarily above 26 kg m^{-3} potential density contour (26-σ_θ isopycnal). The main core of equatorward interior flow appears between approximately 150°E and 140°W at 9°N. East of 140°W, the communication between the extratropics and tropics is largely broken by the potential vorticity barrier, although an intense equatorward flow still appears near the upper pycnocline between 100° and 110°W. At 9°S, because of the lack of a potential vorticity barrier in the Southern Hemisphere, the largest equatorward interior flow can extend from 160° to 90°W. The interior STC transport is estimated by integrating the meridional velocity vertically from 50 m to a depth of 26 σ_θ (potential density = 26 kg m^{-3}) and zonally from the eastern edge of the western boundary current to the eastern boundary (140°E–80°W at 9°N and 160°E–80°W at 9°S). The westernmost longitudes of integration are several hundred kilometers away from the western boundary, which avoided strong boundary currents and their recirculations. We have examined the sensitivity of the interior STC transport using different isopycnal depths and obtained qualitatively similar results from 26 to 26.5 σ_θ. The unfiltered time series of interior STC transport across 9°S and 9°N and the convergence of volume transport into 9°S–9°N are shown in Fig. 2. The meridional transport (Fig. 2a) is mostly negative at 9°N and positive at 9°S, indicating the equatorward interior STC transport. The time-mean transport at 9°S [15.47 Sv (1 Sv ≡ 10^6 m^3 s^{-1})] is more than 3 times larger than that at 9°N (−4.77 Sv). The convergence of interior STC transport (transport at 9°S minus transport at 9°N) (Fig. 2b) averaged in time is 20.2 Sv, indicating the volume transport from the extratropics into the tropics by the convergence of interior STC transport. Further, the time series of transport at 9°S and 9°N and their convergence show strong interannual variability in both hemispheres.

In Fig. 3, the time series of the interior STC transport convergence anomaly between 9°N and 9°S (black line) is compared with the averaged SST anomaly over the central and eastern equatorial Pacific (9°S–9°N, 180°–90°W; red dashed line) where equatorial upwelling is most

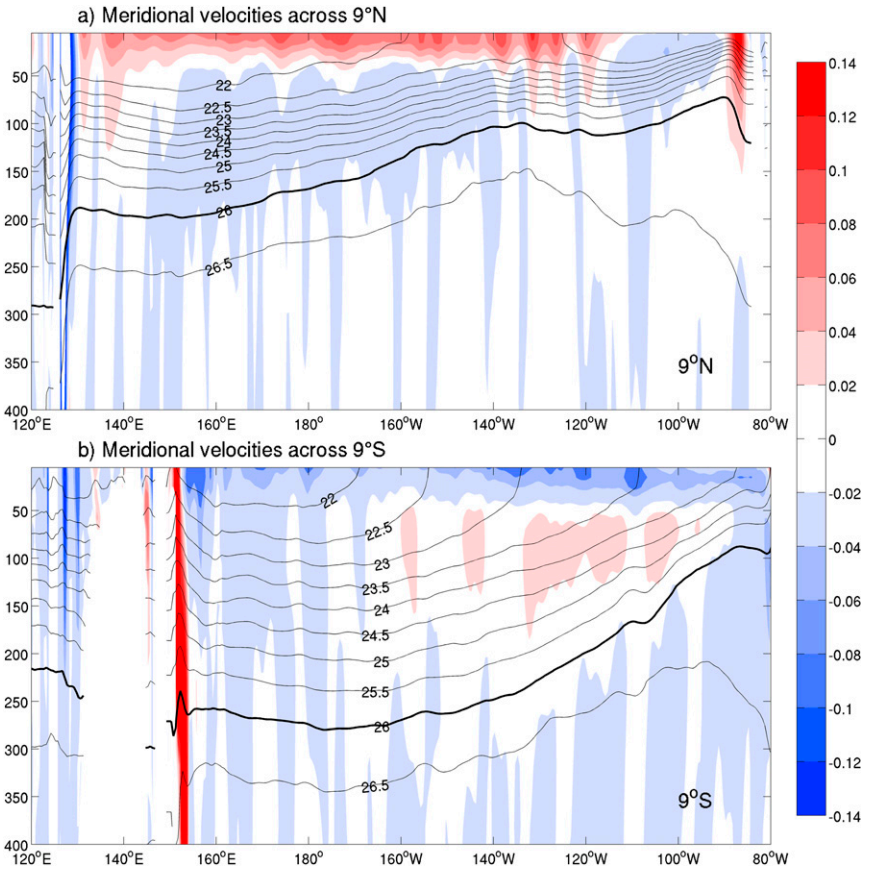

FIG. 1. Longitude–depth sections of time-mean meridional velocity (shading; $m\,s^{-1}$) and isopycnals (black lines; $kg\,m^{-3}$) at 9°N and 9°S from 1960 to 2010. The thick black lines indicate the lower boundary of the STCs (26-σ_θ isopycnal). The unit for depth on the y axis is meters.

intense. The SST index is consistency with the Niño-3.4 index and the results do not change if we use the Niño-3.4 index. Figure 3a shows the unfiltered interior STC transport convergence and SST, and Fig. 3b shows the filtered time series of transport and SST at interannual time scales. Note that the SST is shown with its sign reversed for ease of comparison with the transport. The two time series are clearly anticorrelated, indicating that the stronger (weaker) convergence of mass transport is associated with lower (higher) SST. In particular, an anomaly of 1 Sv of net STC transport convergence corresponds approximately to 0.1°C of SST change. A lagged cross-correlation function indicates that the maximum correlation coefficient is −0.93 when SST leads interior STC transport convergence by 2 months at interannual time scales. This relationship between SST and interior STC transport will be discussed in the next section.

4. Relationship between interior STCs and SST

In this section, we examine the relationship between SST and interior STC transport by calculating the lag correlation between SST anomalies averaged within the central and eastern Pacific (9°S–9°N, 180°–90°W) and the convergence of interior STC transport zonally integrated from 100°W westward to various longitudes. The choice of 100°W as the starting point of the transport integral is based on the finding that the meridional transport east of 100°W is sensitive to local wind forcing and reflective waves (Alexander et al. 2012). Our aim is to discuss the response of meridional transport to the large-scale pattern of wind stress forcing directly associated with tropical SST. The correlation is shown in Fig. 4. Maximum anticorrelation exists between the interior STC transport convergence zonally integrated across the basin and SST with the latter leading ~3–4 months. However, the interior STC transport convergence in the eastern part is positively correlated with SST with the latter leading ~3–4 months. To further examine the two different relationships, we separate the interior STC transport convergence into the western region (160°E–130°W) and the eastern region (130°–100°W). The SST is highly correlated with the western interior STC transport convergence with the highest

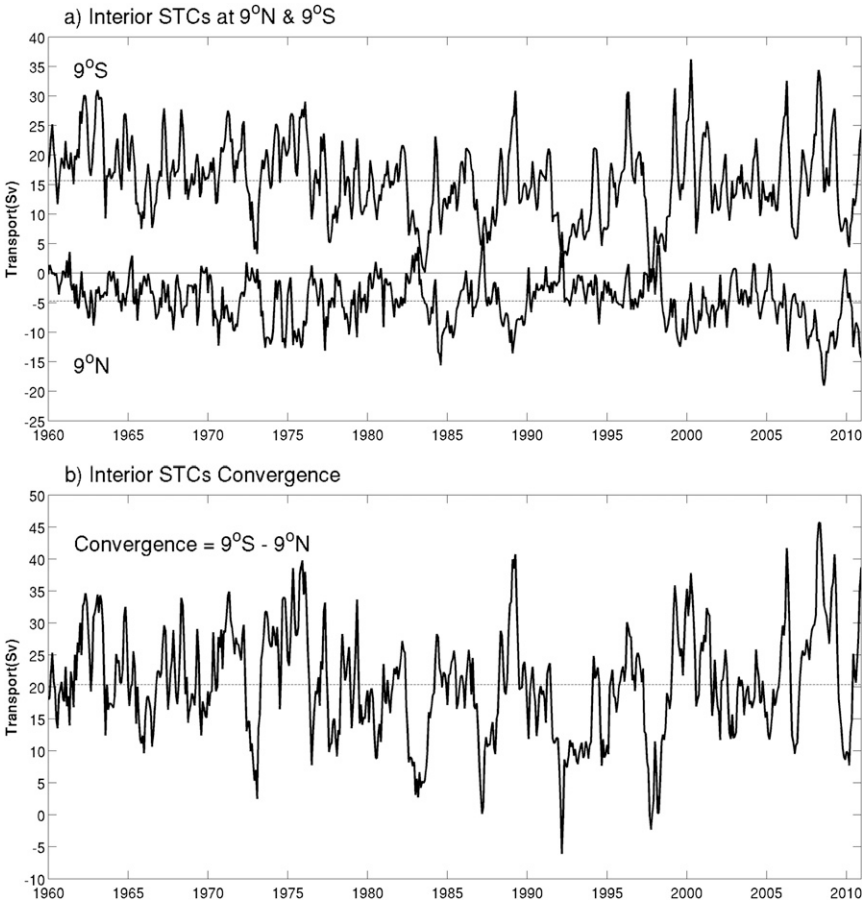

FIG. 2. Unfiltered time series of interior STC transport that is defined as the integrated meridional velocity from 50 m to a depth of 26 σ_θ at (a) 9°N and 9°S and (b) their convergence. The horizontal dashed lines indicate the mean value of each time series from 1960 to 2010.

correlation of −0.90 when the SST leads the transport convergence by 3 months, and a secondary maximum correlation of +0.61 when the SST lags transport by 17 months (Fig. 5a). In contrast, the highest correlation here is only +0.33 when the SST leads the transport convergence by 6 months (Fig. 5b). These results indicate that the significant correlations between the SST and interior STC transport convergence occur only in the western part of transport, not in the eastern one.

The different relation of the interior STC transport in the eastern and western regions to the equatorial SST anomaly results from the opposite sign of the wind anomalies when an ENSO event occurs. This structure of wind stress is consistent with the heat-induced circulation described by Gill (1982). During the developing phase of an El Niño event, the dominant surface westerly wind anomalies over the central Pacific induce divergence of the western interior STC transport, while the weak surface easterly wind anomalies still occur in the far eastern Pacific, which has a much weaker influence on the STC transport convergence than the western one. These wind anomalies with opposite directions in the eastern and central Pacific cause a different interior STC transport convergence response.

This physical relationship can be further clarified from the correlation maps of SST and zonal wind stress with the reference time series of the western (Fig. 6) and eastern (Fig. 7) interior STC transport convergence, respectively. The correlation patterns of SST with the western cell convergence resemble the associated patterns of canonical ENSO (Fig. 6a). In particular, the large negative correlation within 10°S–10°N, 160°W–160°E in Fig. 6b reveals the major area of zonal wind anomalies, which force the interior STC transport convergence changes associated with the ENSO events. Figure 7a shows that the correlation patterns of SST with the eastern interior STC also resemble the ENSO oscillation, but of an opposite phase with the correlation patterns shown in Fig. 6 and of much weaker amplitude. The above results indicate that SST evolution associated

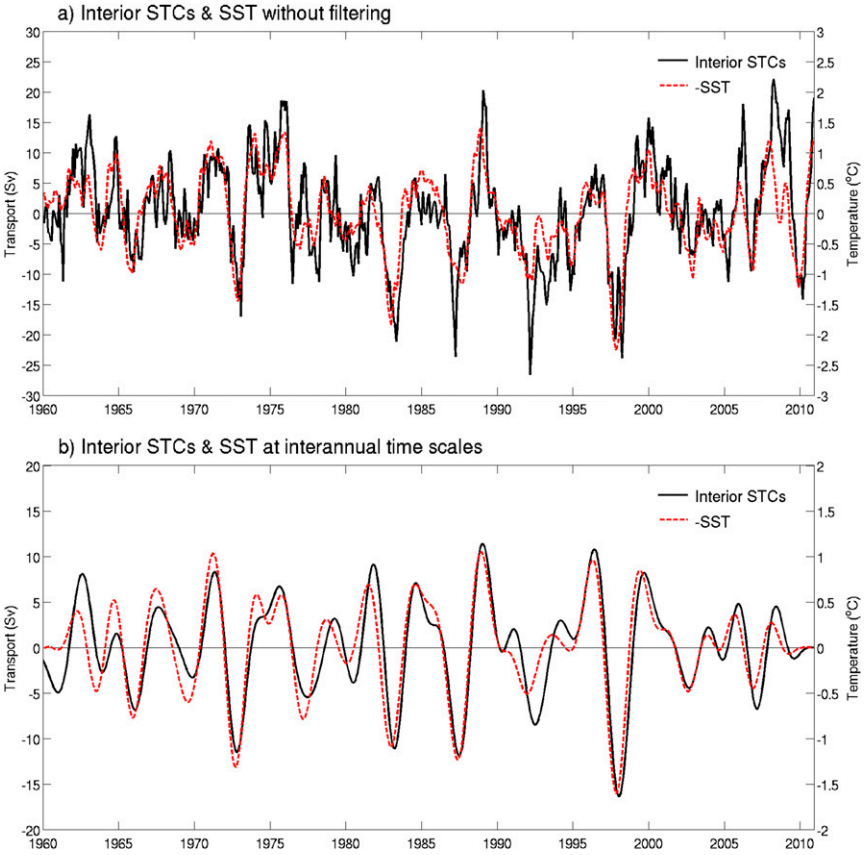

FIG. 3. Monthly anomalies of interior STC transport convergence between 9°N and 9°S (black line) and averaged SST over the central and eastern equatorial Pacific (9°S–9°N, 180°–90°W; red dashed line) (a) without filtering and (b) with interannual bandpass filtering. SST is shown with the sign reversed for ease of comparison.

with ENSO is more strongly related with the western interior transport convergence but is not significantly correlated with eastern interior transport convergence. In fact, the direction of meridional transport in the eastern equatorial Pacific is somewhat opposite from that in the central equatorial Pacific. The overall relationship between SST and interior STC transport convergence is further examined below in light of the recharge–discharge mechanism.

5. Recharge–discharge process by correlation analysis

In this section we further study the corresponding process in the context of the recharge–discharge theory formulated by Jin (1997a,b) and evaluated by Meinen and McPhaden (2000, 2001). First, we set a box in the equatorial Pacific (Fig. 8) to discuss the relationships between equatorial SST, WWV, and mass transports convergence. The interior STC transport is defined as the integrated meridional transport (red line), zonally from 140°E to 80°W and from 160°E to 80°W for 9°N and 9°S, respectively, and vertically from 50 m to a depth of 26 σ_θ. The longitudinal range includes both the western and eastern parts discussed in section 4 because the analysis in this section aims to examine meridional mass transport over the whole basin, which affects the basinwide recharge–discharge process. In addition, we define the total STC transport as the meridional transport vertically integrated from the surface to a depth of 26 σ_θ and the same zonal integration (red line) as interior STC transport. The total STC transport includes the interior STC transport and the Ekman transport. However, the interior STC transport is much larger than the Ekman transport (not shown), and thus the inclusion of Ekman transport does not cause any phase shift.

We also define the ''western boundary transport'' as an integrated meridional transport vertically from the surface to a depth of 26 σ_θ and zonally from the western boundary (the east coast of Mindanao for 9°N and New Guinea for 9°S) to 140°E at 9°N and 160°E at 9°S (blue line). The separation longitudes are chosen so as to

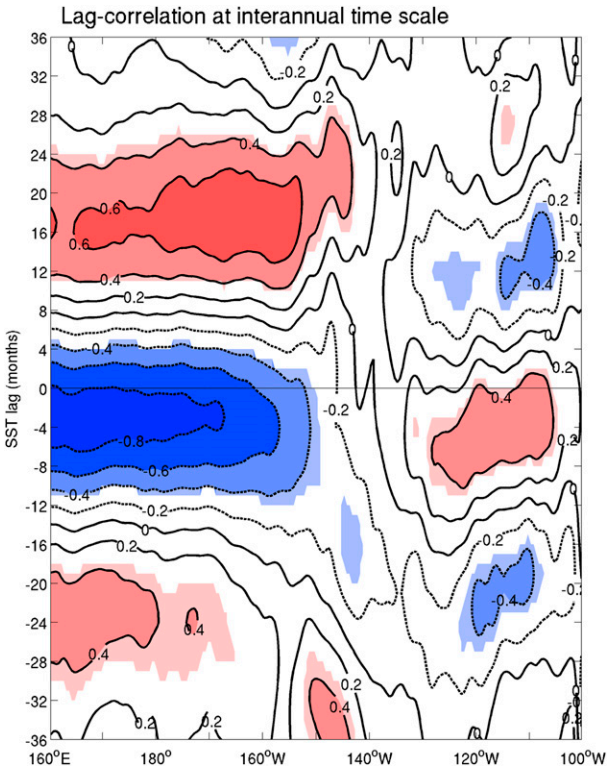

FIG. 4. Lag correlation between the SST anomaly averaged over the central and eastern equatorial Pacific (9°S–9°N, 180°–90°W) and the convergence of interior STC transport anomalies across 9°S and 9°N zonally integrated from 100°W westward to various longitudes at interannual time scales. Positive (negative) values in *y* axis indicate that the SST anomaly lags (leads) the STC anomaly by month. The shaded areas indicate significance at the 95% confidence level (correlations greater than 0.32). Contour lines are drawn every 0.2.

include the possible tight recirculation cells of the boundary currents. The wind stress curl index is calculated as the difference between the zonally integrated wind stress curl at 9°N (140°E–80°W) and 9°S (160°E–80°W), which is proportional to the divergence of the Sverdrup transport in the equatorial zone. The equatorial SST is averaged over the central and eastern equatorial Pacific (9°S–9°N, 180°–90°W; hatched area). Previously, the WWV was generally defined as the volume of water warmer than 20°C over the equatorial region, where the 20°C isotherm was chosen to approximate the thermocline (Meinen and McPhaden 2000, 2001). Although it is more natural to calculate a volume above a certain isopycnal, there were no available long records of salinity in the tropics for calculating the isopycnal WWV in previous studies. Here, we use SODA assimilated temperature and salinity to better define the WWV as the volume of water above 26.0 kg m^{-3} isopycnal in the box (9°S–9°N, 120°E–80°W). We also calculate the Indonesian Throughflow (ITF) as the meridional transport integrated vertically from the surface to a depth of 26 σ_θ and zonally from 120° to 140°E. The transport anomalies of ITF are anticorrelated with the convergence of interior STC transport (not shown). However, the amplitude of ITF anomalies is much smaller than both convergences of the interior STC transport and the western boundary transport (the standard deviations are 0.97, 5.22, and 5.15 Sv for the ITF and the convergences of the interior STC transport and western boundary transports, respectively). Therefore, we neglect the ITF contribution to the recharge–discharge process in our study.

In Fig. 9 the total STC transport (black line) is compared with the western boundary transport (red dashed line) across 9°S and 9°N. The total STC transport is generally anticorrelated with the western boundary transport. This strong anticorrelation between boundary transport and total STC transport has been noted in both realistic and idealized model simulations (Springer et al. 1990; Lee and Fukumori 2003; Hazeleger et al. 2004; Wang et al. 2003; Ishida et al. 2008). However, the relationship between total STC transport and boundary transport exhibit different behaviors in the Northern and Southern Hemispheres. In the Northern Hemisphere (Fig. 9a), the amplitude of the total STC transport is larger than that of the western boundary transport (standard deviation is 4.47 and 2.46 for the former and the latter, respectively). Although the total STC and the boundary transports tend to compensate for each other, there is a shift of several months between their peaks (the simultaneous correlation coefficient is only −0.54). As a result, there is a significant net meridional transport (total STC plus western boundary transports) across 9°N into the box. In contrast, Fig. 9b shows that the western boundary transport largely compensates for the total STC transport in the Southern Hemisphere (the simultaneous correlation coefficient is −0.96) and their amplitudes are similar (standard deviation is 4.43 and 4.53 for the total STC and western boundary transports, respectively) so that the net meridional transport across 9°S is small. Furthermore, the convergence of net meridional transport is correlated with that of the total STC transport at 0.83 (Fig. 10) while its correlation with the convergence of the western boundary transport is only −0.51. Therefore, the convergence of net meridional transport is dominated by the total STC transport convergence (or the interior STC transport convergence), instead of the western boundary transport convergence.

In the previous section we showed that the equatorial SST is correlated with the interior STC transport convergence with the highest correlation of −0.93 when

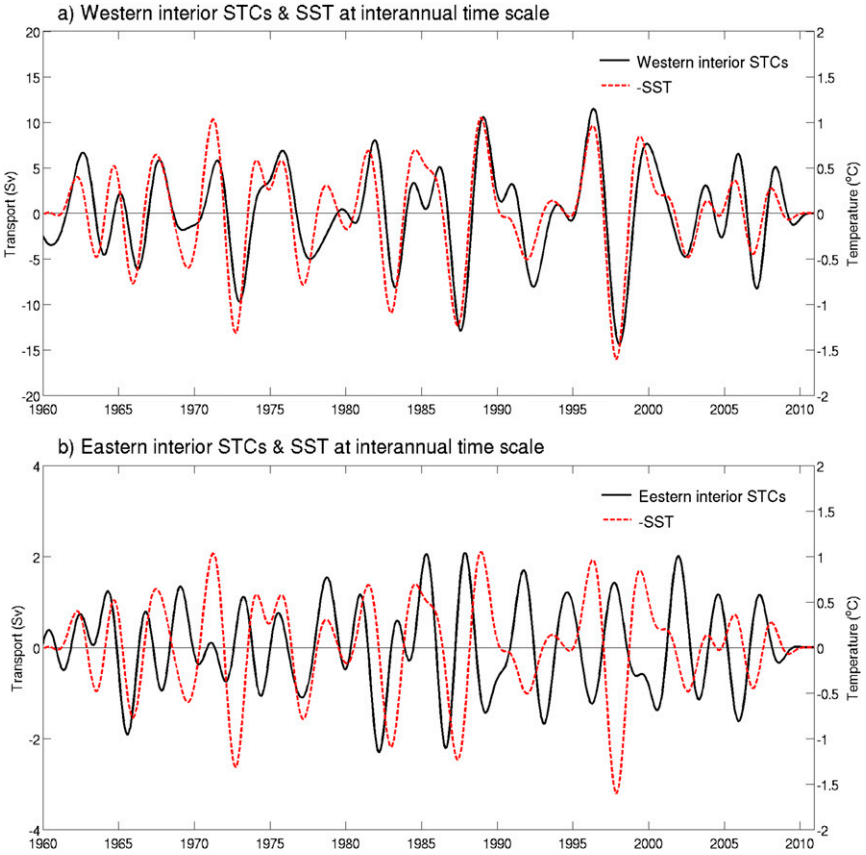

FIG. 5. Monthly anomalies of (a) western interior STC transport convergence (160°E–130°W; black line) and (b) eastern interior STC transport convergence (130°–100°W; black line) and averaged SST over the central and eastern equatorial Pacific (9°S–9°N, 180°–90°W; red dashed lines) at interannual time scales. SST is shown with the sign reversed for ease of comparison.

SST leads the transport by 2 months, and a positive correlation of +0.59 when the transport convergence leads SST by 18 months (Fig. 3b). We further estimate the relationship between tropical SST and WWV in Fig. 11a at interannual time scales. The SST is also highly correlated with WWV, having the highest correlation of −0.84 when SST leads WWV by 10 months and another extremum (coefficient +0.73) when SST lags by 10 months. Furthermore, Fig. 11b shows the relationship between the wind stress curl index and SST. The wind stress curl index is highly correlated with SST when SST leads by 2 months, indicating that the wind stress curl and interior STC transport convergence are simultaneous.

The above results reveal that the interior STC transport convergence is caused by the negative wind stress curl index before the warm SST phase, deepening the thermocline depth across the equatorial Pacific (WWV). This process can be viewed as the recharge process of the zonal-mean equatorial heat content (Wyrtki 1985; Jin 1997a). This recharge process leads to a deepened thermocline that allows warmer water to be pumped into the surface layer by climatological upwelling. As a result, the SST in the central and eastern equatorial region turns into a warm phase. Following the peak of a warm phase, the positive wind stress curl index causes the interior STC transport to diverge, leading to the following discharge process. The discharge leads the whole equatorial Pacific thermocline (WWV) to shoal. This decreased WWV allows colder water to be pumped into the surface layer by climatological upwelling and the SST turns into a cold phase (Jin 1997a).

The corresponding time intervals for the different stages from the recharging stage to the discharged stage are determined by summarizing the lagged months of maximum correlations between the SST index and other key variables, including the interior STC transport convergence, WWV, and wind stress curl index shown in Fig. 12. The essential sequence of the processes, as well as their interconnections, is summarized in Fig. 13. This schematic representation of the evolution of El Niño events is modified from Jin (1997a). The evolution of the

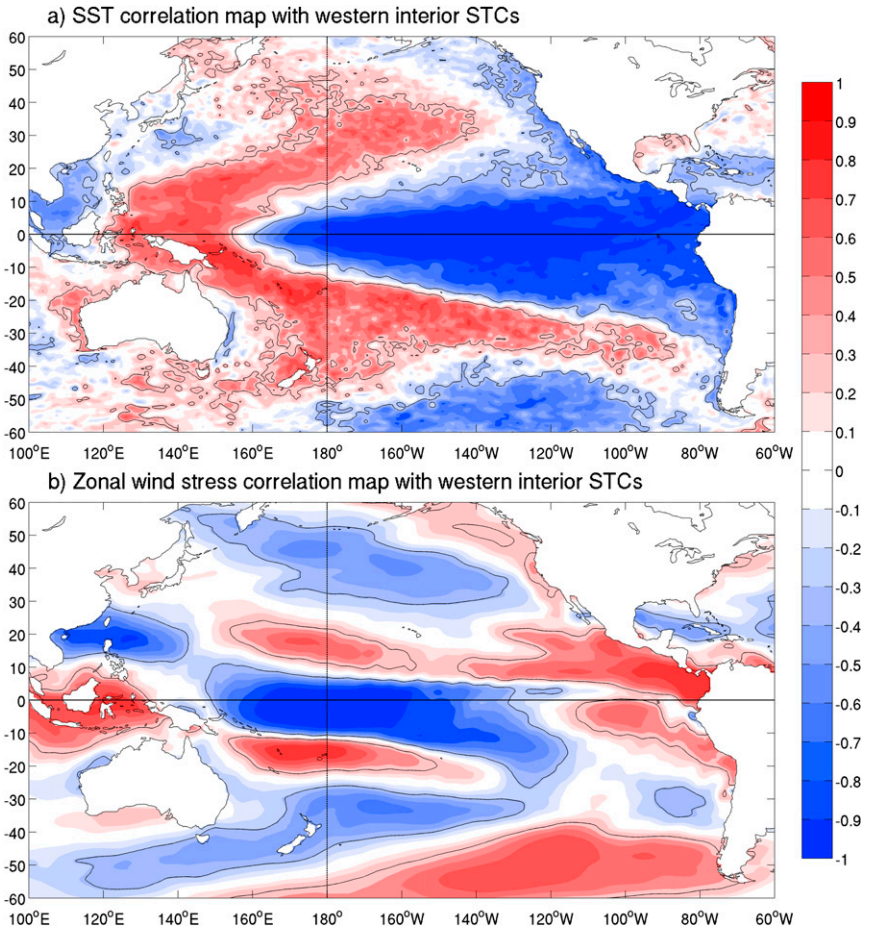

FIG. 6. The spatial distribution of temporal correlation between the referenced time series of western interior STC transport convergence and the time series of (a) SST and (b) zonal wind stress at each grid point with transport lagging SST and wind stress by 3 months. Correlations greater than 0.31 are significant at the 95% confidence level (black contours).

El Niño events starts from the recharging stage (maximum interior STC transport convergence; stage I), develops to the recharged stage (maximum WWV; stage II), peaks at the warmest SST stage (stage III), is followed by the discharging stage (maximum interior STC transport divergence; stage IV), and finally reaches the discharged stage (minimum WWV; stage V). The lagged months of maximum correlation, as found in Fig. 12, give corresponding time intervals of 8, 10, 2, and 8 months for the transition from stage I to II, stage II to III, stage III to IV, and stage IV to V, respectively. Since the results are based on a linear correlation analysis, the same time lags can be applied to La Niña evolution. We have conducted the same analysis but using 7°S and 7°N for the calculation of meridional transport instead of 9°S and 9°N. The results are similar to that along 9°S and 9°N.

The above time intervals of ENSO evolution can be determined by the adjustment time of tropical Pacific oceanic waves. The evolution of WWV is explained by the off-equatorial Sverdrup transport associated with the Rossby waves (Jin 1997a). Bosc and Delcroix (2008) also found that observed equatorial Rossby waves (first baroclinic, first meridional) were responsible for changing the basin-scale zonal pressure gradient and consequently the anomalous meridional geostrophic transports of warm water. An and Kang (2000) used a simple coupled model, which externally includes the equatorial wave dynamics represented by the Kelvin and gravest Rossby waves to analyze the adjustment processes in the context of the recharge oscillator. In their result, the zonal-mean thermocline depth leads the SST by a quarter-cycle but also lags the SST by a quarter-cycle (their Fig. 2). Furthermore, the interior meridional transport leads the SST by about 150° and also lags the SST by about 20° in phase (their Fig. 3). With an average ENSO oscillation at 40 months, An and Kang's result dictates

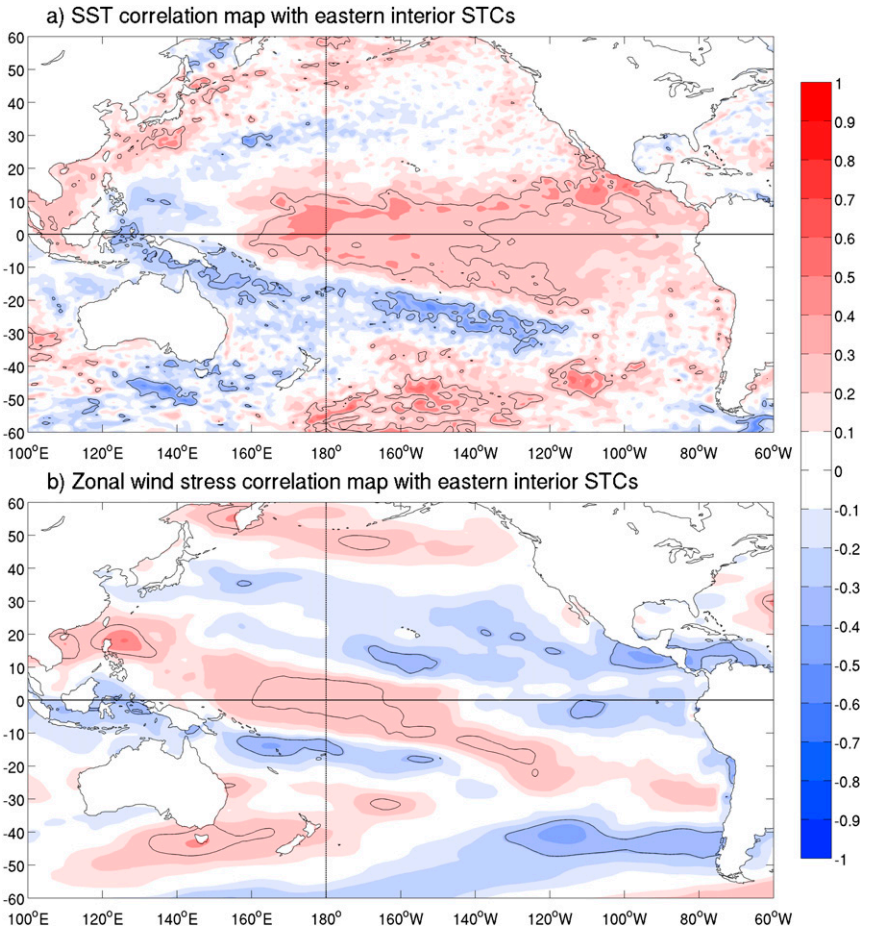

FIG. 7. As in Fig. 6, but for the eastern interior STC transport convergence lagging SST and wind stress by 6 months.

that the zonal-mean thermocline depth leads the SST by 10 months and lags the SST by 10 months, and the interior meridional transport leads the SST by about 17 months and lags the SST by about 3 months. The above time intervals are consistent with our results summarized in Figs. 12 and 13.

Although previous theoretical works have speculated that the zonal equatorial wind anomalies (e.g., Jin 1997a; Clarke et al. 2007) in the central and western Pacific play important roles in modifying the mean equatorial thermocline depth (i.e., the warm water volume), the specific processes involved are generally parameterized. Jin (1997a) argued that Sverdrup transport either pumping the mass in or out of the equatorial region depended on wind forcing and assumed that the effect of this process on the tendency of the thermocline depth in western equatorial Pacific is proportional to the zonally integrated wind stress in the equatorial band [his Eq. (2.3)]. He sets the proportional coefficient as 4 months. On the other hand, Clarke et al. (2007) argued that the wind stress curl effects on both sides of the equator should be explicitly taken into account. Moreover, since the change of the isopycnal surface stretches the vortex tube, the transport process is not strictly in Sverdrup balance. In both Jin (1997a) and Clarke et al. (2007), however, the subsurface geostrophic meridional transport is not explicitly represented and its contribution to the time tendency of the equatorial WWV is largely parameterized with tunable parameters to represent its time scale. Our results provide further insights into this process by providing a specific time interval. This information may be useful in further refining these theoretical models and in examining the coupled ocean–atmosphere general circulation model (CGCM) simulations.

6. Composites of ENSO events

In the last section, we used correlation analysis to quantify the relations between bandpass-filtered WWV, mass transport, and equatorial SST. The approach works

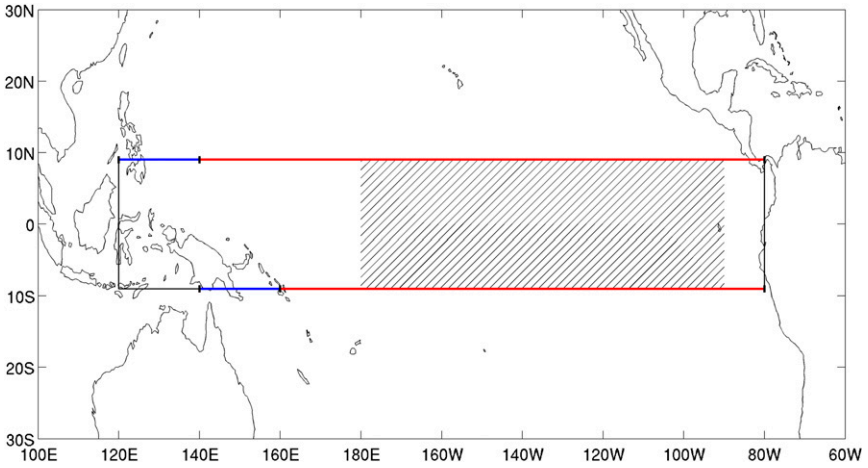

FIG. 8. The box in the equatorial Pacific Ocean used to analyze recharge–discharge process. The WWV is calculated over the area between 9°S and 9°N, extending longitudinally from 120°E to 80°W . The interior STC transport is zonally integrated from 140°E to 80°W along 9°N and 160°E to 80°W along 9°S (red lines). The western boundary transport is zonally integrated from the western boundary (the east coast of Mindanao for 9°N and New Guinea for 9°S) to 140°E at 9°N and 160°E at 9°S (blue lines). The wind stress curl index is calculated as the averaged wind stress curl along 9°N (140°E–80°W) minus along 9°S (160°E–80°W). The equatorial SST is averaged over the central and eastern equatorial Pacific (9°S–9°N, 180°–90°W; hatched area).

well for finding repeating cycles, but the evolution of ENSO sometimes exhibits an episodic rather than a cyclic nature (Kessler 2002). As a result, the periodicity in those ENSO events can be quite irregular. To ensure the robustness of our result, a composite analysis is performed from selected events for El Niño–developing and La Niña–developing phases separately to further examine the recharge–discharge process. These events are selected based on monthly time series of SST averaged in the region 9°S–9°N, 180°–90°W°. The climatological annual cycle and linear trend are removed from the time series to form SST anomalies. A 5-month running average is further applied to the SSTA time series to form the SST index for the composite analysis. Only strong interannual oscillations with an amplitude of SST index larger than one standard deviation are considered. Events with a clear evolution from cold to warm phase are selected as the El Niño–developing phase. The events selected include 1963/64, 1965/66, 1968/69, 1972/73, 1982/83, 1987/88, 1991/92, 1997/98, 2002/03, 2006/07, and 2009/10. Those events with a clear evolution from warm to cold phase are selected as the La Niña–developing phase. The events selected include 1964/65, 1970/71, 1973/74, 1984/85, 1988/89, 1998/99, and 2007/08.

Using the month of SST transition from cold to warm phases or vice versa as the reference time, the evolution of equatorial SST, interior STC transport convergence, and WWV from each event of the El Niño–developing and La Niña–developing phases are shown in Fig. 14 (blue lines). Their composite evolutions are also shown (red line). In most El Niño–developing events, the SSTA in the cold phase is weaker than that in the warm phase, and the corresponding cold phase lasts longer (~2 yr) before entering the warm phase (Fig. 14a). SSTA in the cold phase generates persistent convergence of interior STC transport (Fig. 14b). The transition of the composite interior STC transport from convergence to divergence occurs 2–3 months after the SST phase transition, consistent with the previous result that the interior STC transport lags SST by 2 months. The convergence of interior STC transport recharges the tropical upper ocean to increase the WWV before the peak of El Niño (Fig. 14c). In most El Niño–developing events, the WWV shows two peaks corresponding to the double peaks in SSTA and interior STC transport convergence in the cold phase.

In La Niña–developing events, the SSTA in the warm phase before a mature La Niña is larger than the SSTA in the cold phase (before a mature El Niño in magnitude); however, the warm phase in La Niña–developing events last only 17 months on average, shorter than the persistent cold phase in El Niño–developing events (Fig. 14d). In addition, the transition of the SSTA from warm to cold phase leads the transition of interior STC transport from divergence to convergence by 2 months (Fig. 14e). The interior STC transport divergence in the warm phase leads to the decrease of WWV before the peak of La Niña (Fig. 14f). The minimum WWV cycle

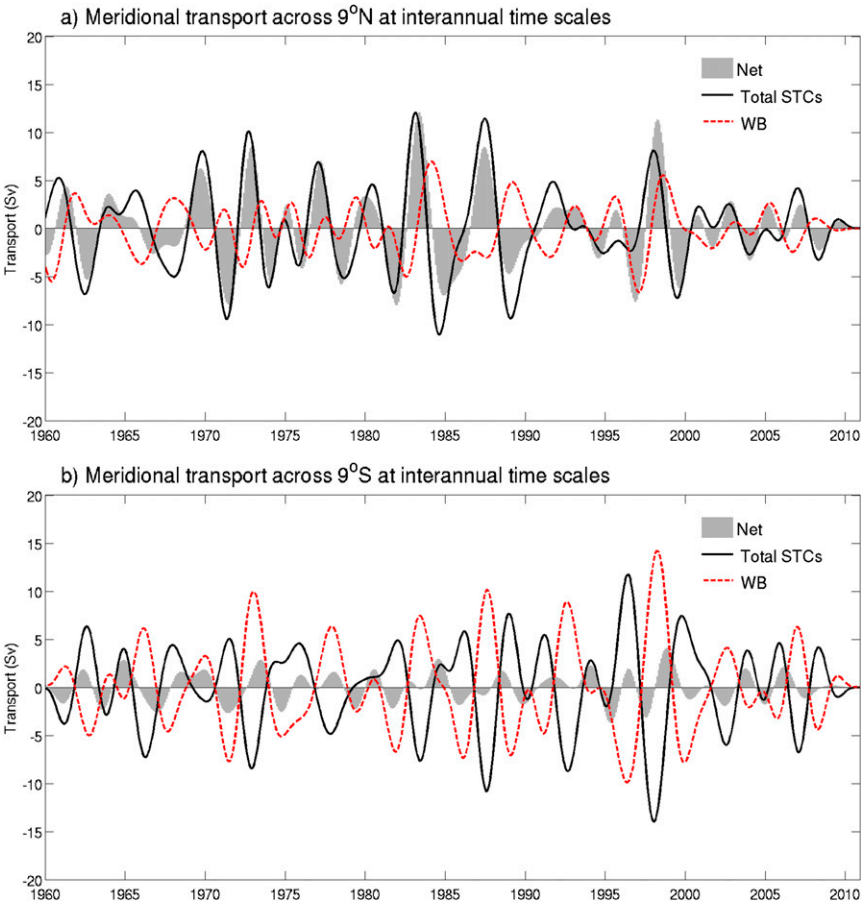

FIG. 9. Monthly anomalies of the western boundary transport (red dashed lines), total STC transport (black lines), and net meridional transport (western boundary transport plus total STC transport; gray shading) across (a) 9°N and (b) 9°S at interannual time scales.

corresponds to the zero SSTA in the composite SST cycle (a quarter-cycle phase difference).This phase difference corresponds to an 8-month interval assuming a typical period of the ENSO cycle as 32 months. The 8-month period also corresponds well to the period between minimum WWV and minimum SSTA of the composite cycle in Figs. 14f and 14d.

Here we calculate the time interval between each stage in the recharge–discharge process based on composite results. From El Niño–developing events in Figs. 14a–c we find that the peak of interior STC transport convergence (stage I), maximum WWV (stage II), and warm SSTA (stage III) are from −2 to −10, +2, and +8, respectively, and that the time intervals between stages I, II, and III are 4–12 and 6 months. We can also determine the time intervals between the peaks of warm SSTA (stage III), interior STC transport divergence (stage IV), and minimum WWV (stage V) from La Niña–developing events in Figs. 14d–f, which are −6, −4, and 0, respectively. The result indicates that the time intervals between stages III, IV, and V are 2 and 4 months. The recharge–discharge processes revealed in the composite evolution of different ENSO events are consistent with the conclusions obtained from the correlation analysis, and the corresponding time intervals in the composite ENSO evolution from stages I through V are 4–12, 6, 2, and 4 months.

Note that the composite evolution reveals a temporal asymmetry characterized by a longer recharge process in the cold SST phase and a shorter discharge process in the warm SST phase. The asymmetry has been attributed to a couple of reasons. One explanation is the nonlinear atmospheric response to the SST distribution in the equatorial Pacific and the surrounding tropical Pacific and Indian Ocean such that surface wind forcing in the far western equatorial Pacific tends to efficiently terminate the warm phase into the La Niña condition, but to prolong the cold phase before the El Niño condition (Kug and Kang 2006; Ohba and Ueda 2009; Ohba and Watanabe 2012; Okumura and Deser 2010; Okumura

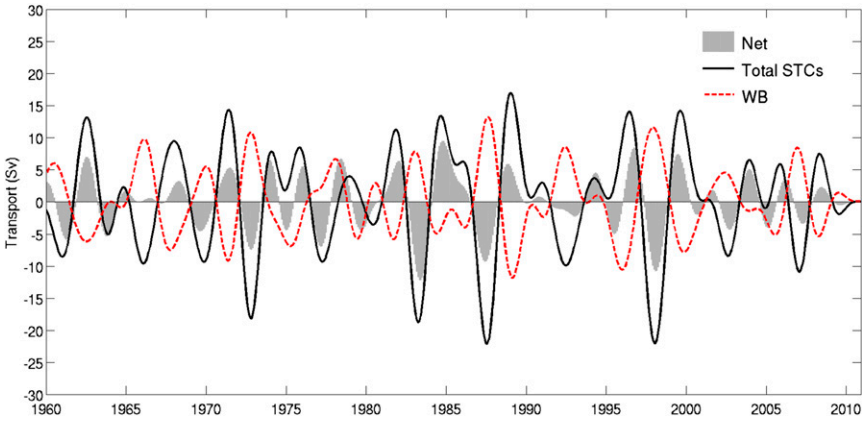

FIG. 10. Monthly anomalies of western boundary transport convergence (red dashed line), total STC transport convergence (black line), and net meridional transport convergence (western boundary transport plus total STC transport; gray shading) at interannual time scales.

et al. 2011). Nagura et al. (2008) indicated that the interannual variation of tropical instability waves (TIWs) slows down the transition from La Niña to El Niño but does not to work from El Niño to La Niña. Another explanation was provided by Hu et al. (2014) who argued that the persistence of the cold condition is related to the equatorial upwelling Kelvin waves and the reflected Rossby wave in stronger La Niña events.

7. Asymmetry of interior STC transport

In Fig. 9, our results indicated a strong asymmetry of the interior STC transport in the Southern and Northern Hemispheres. The results also indicate the difference of the relationships between the western boundary transport and the interior STC transport. The difference is particularly evident during some strong El Niño events (i.e., 1972/73, 1976/77, 1982/83, and 1997/98) in Fig. 9, in which the interior STC transport was compensated by the western boundary transport in the Southern Hemisphere but not in the Northern Hemisphere. The noncompensation in the Northern Hemisphere was caused by the phase lag of the interior STC transport and western boundary transport as mentioned in the study by Ishida et al. (2008). Their study found that the north–south asymmetry of the transport is related to the southward migration of the westerly wind when El Niño events reach their peak amplitude (Harrison 1987; Harrison and Larkin 1998; Harrison and Vecchi 1999; Larkin and Harrison 2002; Vecchi and Harrison 2003; Lengaigne et al. 2006; McGregor et al. 2012; Stuecker et al. 2013).

Actually, the southward shift of the westerly wind results in not only the north–south asymmetry of the western boundary transport but also the north–south asymmetry of the interior STC transport. Figure 15 shows the time series of the composite interior STC transport and western boundary transport at 9°S and 9°N of the El Niño events in 1972/73, 1976/77, 1982/83, and 1997/98. These four events are selected because of the clear southward shift of westerly wind anomaly (McGregor et al. 2012; Stuecker et al. 2013). Year (0) corresponds to the developing period of El Niño events (1972, 1976, 1982, and 1997) and year (+1) corresponds to the decaying periods (1973, 1977, 1983, and 1998). In the Northern Hemisphere, the western boundary transport turns anomalously northward near the end of year (0), about 6 months after the interior STC transport turns anomalously northward near April (0). In contrast, the interior STC transport in the Southern Hemisphere is well compensated by the western boundary transport. The result is consistent with Ishida et al. (2008). Furthermore, the discharging of interior STC transport at 9°N terminates earlier than its counterpart does at 9°S. That is, the discharge at 9°N turns to recharge in the year (+1) summer, while the discharge at 9°S persists beyond year (+1). To explain the long persistent time of discharging at 9°S, we show in Fig. 16 the composite maps of wind forcing and the depth of the 26-σ_θ anomaly for the four El Niño events. This figure contains composite maps in developing, mature, and decaying states for the four El Niño events. Note in Fig. 16 that the field of 26-σ_θ depth in the developing and decaying stages (Figs. 16d and 16f) lags the corresponding field of wind forcing (Figs. 16a and 16c) by 3 months. This is based on the time-lagged response of interior STC transport (and WWW) to SST (and wind forcing) in the El Niño–developing and decaying phases (Fig. 14). A near in-phase relation is found between SST and interior STC transport in the mature phase of El Niño.

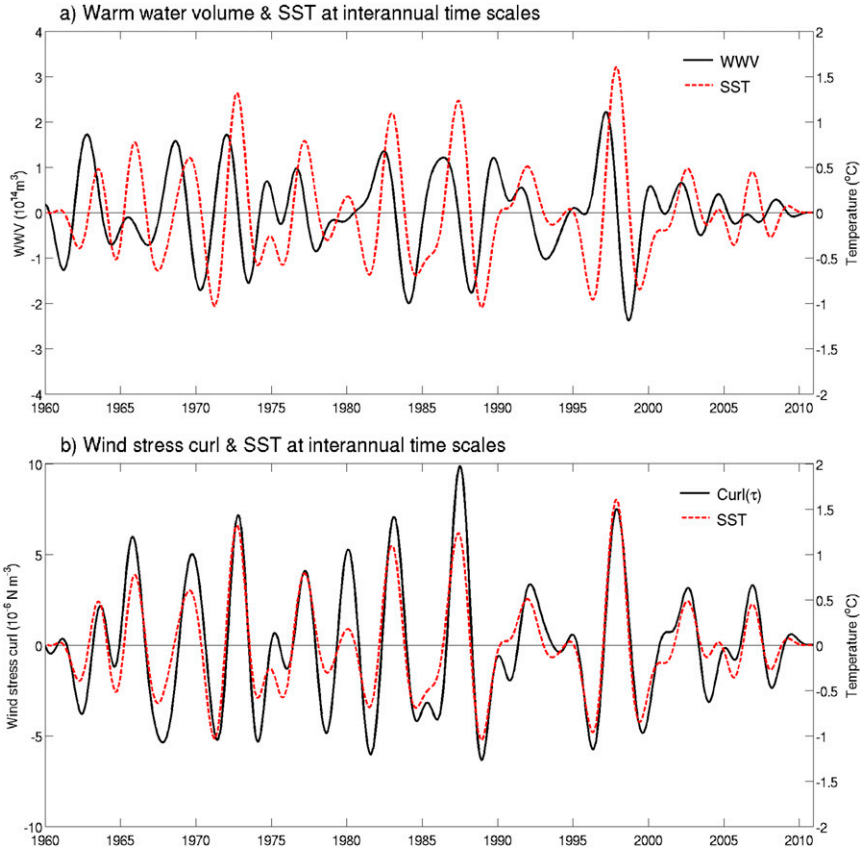

FIG. 11. Monthly anomalies of (a) WWV and (b) wind stress curl index shown by the black lines in comparison with averaged SST over the central and eastern equatorial Pacific shown by the red dashed lines at interannual time scales.

During the developing stage of El Niño, westerly wind anomalies in the western Pacific, and the associated positive wind stress curl in the northwestern Pacific can be seen in Fig. 16a. This wind forcing induces the anomalous shallow interior pycnocline in the western and central North Pacific (Fig. 16d). The anomalously southward transport in the western boundary and anomalously northward interior STC transport at 9°N (Fig. 15) are largely accountable by the geostrophic balance inferred from thermocline depth. As El Niño matures, westerlies develop in the central equatorial Pacific and the pattern of wind stress curl field is symmetric about the equator (Fig. 16b). There are symmetric structures in the depth of 26 σ_θ with two shallow regions located north and south of the equator in the western equatorial Pacific and a deep region in the eastern equatorial Pacific (Fig. 16e). The zonal structure of transports shows that the southern interior STC transport is mainly influenced by currents near the date line, and the contribution from currents near the eastern boundary is negligible (also found in section 4). This structure corresponds to the anomalously northward interior STC transport at 9°N, the anomalously southward interior transport at 9°S, and the anomalously northward transport in the western boundary at 9°S (Fig. 15). In the decaying phase following the mature stage, westerlies move slightly southward along with the corresponding wind stress curl (Fig. 16c). The wind forcing shoals the equatorial thermocline except at the eastern boundary and deepens the thermocline north of the equatorial waveguide (Fig. 16f). The thermocline anomaly pattern corresponds to the anomalously northward transport in the western boundary and near-zero interior STC transport at 9°N due to a phase transition. At the same time, the shallow thermocline depth in the South Pacific indicates the anomalously southward interior transport and the anomalously northward transport in the western boundary at 9°S (Fig. 15). The above-stated evolution of transport in Fig. 15 is speculated as a response to the wind forcing, which shows that the anomalously northward western boundary transport is generated after the anomalously northward interior STC transport at 9°N by half a year. It also explains the termination of discharging of the interior STC transport

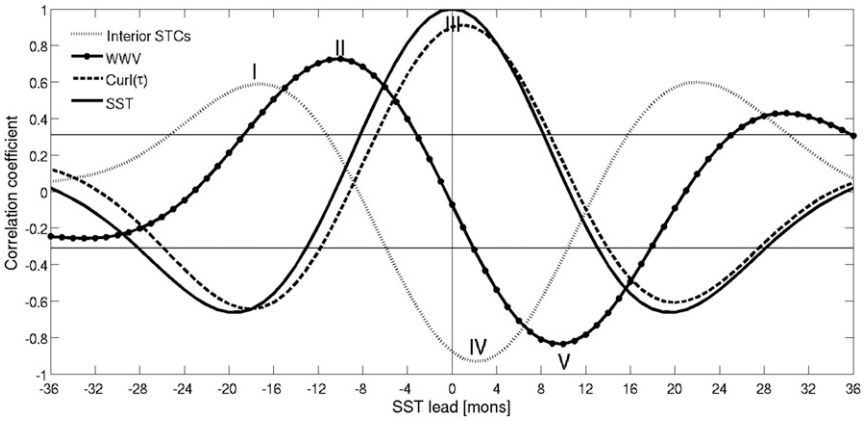

FIG. 12. Lag correlation of SST anomaly with interior STC transport convergence (dotted line), WWV (dashed–dotted line), wind stress curl index (dashed line), and SST (solid line) at interannual time scales [roman numerals (I, II, III, IV, and V) represent the stages in Fig. 13]. The horizontal black lines indicate the minimum value of the correlation coefficient (±0.31) that would be significant at the 95% confidence level.

in year (+1) at 9°N, and the persistent discharging of the interior STC transport at 9°S.

8. Summary and discussion

In this study we use the Simple Ocean Data Assimilation reanalysis version 2.2.4 (SODA 2.2.4) over the period 1960–2010 to examine the variability of Pacific subtropical cells (STCs) and their relationship to equatorial SST. We also repeat the analysis using NCEP Global Ocean Data Assimilation System (GODAS) over the period 1980–2015 to examine the results, and our result is largely consistent with that from the SODA data.

Results show that the magnitude of interior STC transport at 9°S is more than 3 times larger than that at 9°N with the corresponding mean transport of 15.47 and −4.77 Sv. The interior STC transport convergence anomaly across 9°S and 9°N is highly correlated with equatorial SST anomaly such that every 1-Sv interior STC transport convergence corresponds to a 0.1°C SST decrease (negative correlation). An examination of the above correlation at interannual time scales indicates that the correlation is primarily contributed by the interior transport into the central equatorial zone (160°E–130°W), and in contrast, the interior transport into the eastern part (130°–100°W) is positively correlated with SST. This opposite correlation is physically linked to the reversed zonal wind over the equatorial Pacific in response to the ENSO warm SST anomaly.

A further correlation analysis of the interior STC transport convergence, WWV, SST, and wind stress curl across the Pacific basin amplify a sequence of physical links in Jin's (1997a,b) recharge–discharge theory. The highly correlated processes and associated lead–lag time interval are synthesized to provide a more quantitative evidence of the recharge–discharge processes in ENSO evolution. An enhanced meridional western interior STC convergence (stage I) charges the equatorial upper ocean with warm water to produce a peak WWV (stage II) in 8 months. A changed WWV initiates surface warming in the central and eastern equatorial Pacific and a warmest SST anomaly (stage III) is reached 10

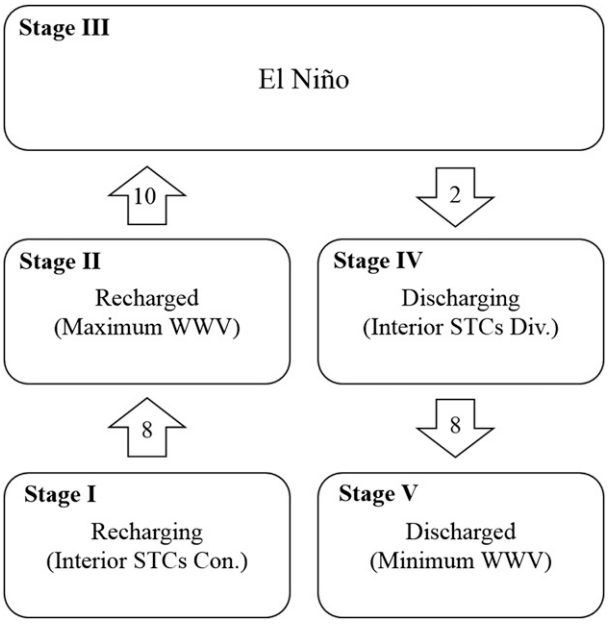

FIG. 13. A schematic representation of the evolution of El Niño events (modified from Jin 1997a) in five stages and with corresponding time lags in months.

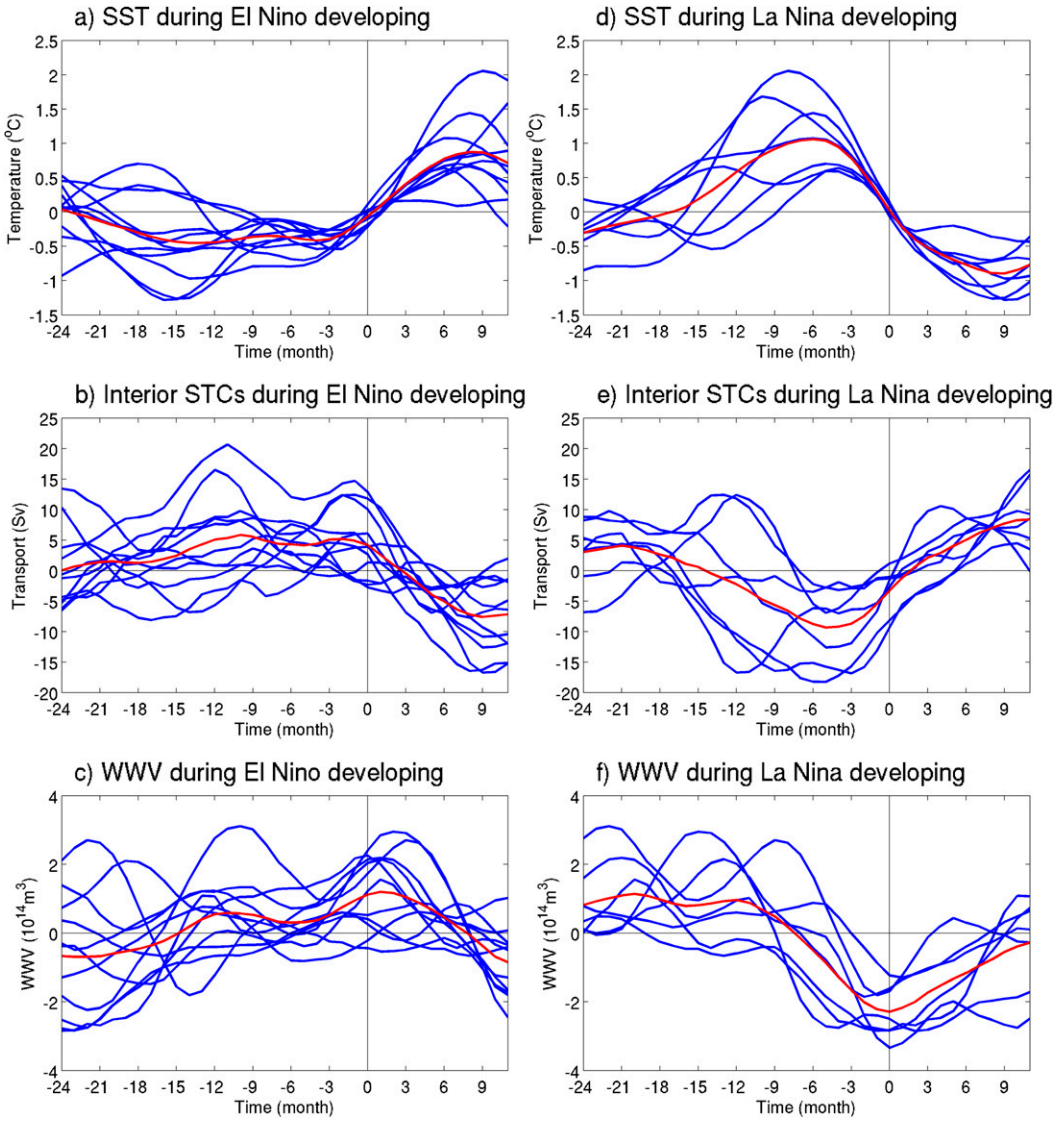

FIG. 14. Temporal evolution of strong interannual oscillations for (a)–(c) El Niño–developing and (d)–(f) La Niña–developing events (blue lines): (a),(d) SST anomalies; (b),(e) interior STC transport convergence anomalies; and (c),(f) the WWV anomalies. All time series are smoothed by 5-month running averages. Evolutions of all events are plotted relative to the SST anomaly transition from cold to warm phase and vice versa. The composite evolutions of the three variables are shown by the red curves.

months after stage II. Atmospheric responses to convective heating over warm SST anomalies result in equatorial westerly wind anomalies and the off-equatorial cyclonic wind stress curl in the western and central Pacific that produce divergence of STC transport. As a result, the divergence of STC transport peaks (stage IV) 2 months after the peak SST. Since a diverging STC transport discharges equatorial warm water, a minimum WWV (stage V) is reached 8 months later. We also examine the recharge–discharge process using composite SST, WWV, and interior STC convergence for 11 El Niño events and 7 La Niña events. The recharge–discharge processes are evident in most events and the evolution time intervals in the composite life cycle are in general agreement with the correlation analysis. An asymmetry of the interior STC transport between the warm and cold episodes is noticed, which is consistent with the asymmetry in the duration of the warm and cold events.

For strong El Niño events, the southward migration of westerly wind anomalies after the mature state of El Niño shoals the thermocline outside the eastern boundary and deepens the thermocline north of the equatorial waveguide. The thermocline anomalies

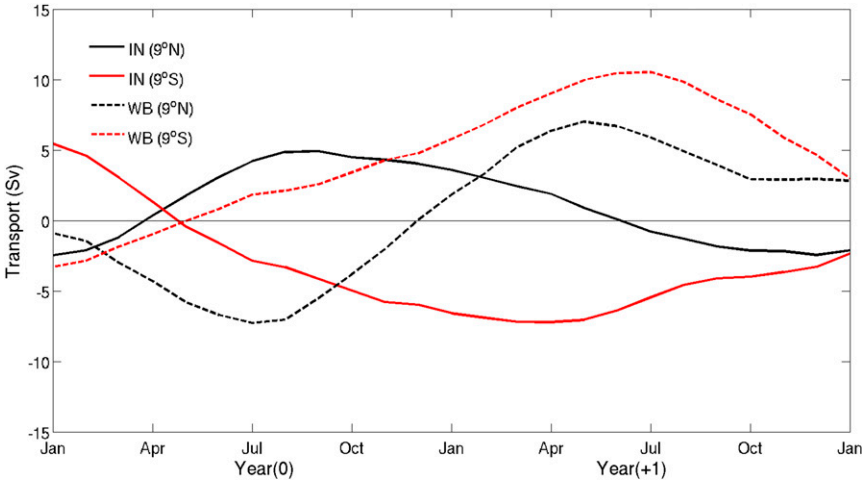

FIG. 15. Time series of the composite interior STC transport (solid lines) and western boundary transport (dashed lines) at 9°S (red lines) and 9°N (black lines) of the El Niño events for 1972/73, 1976/77, 1982/83, and 1997/98. Year (0) corresponds to the developing year of El Niño events (1972, 1976, 1982, and 1997) and year (+1) corresponds to the decaying periods (1973, 1977, 1983, and 1998). All time series are smoothed by 5-month running averages.

correspond to the anomalous northward transport in the western boundary and the near-zero anomalous interior STC transport there along 9°N. In contrast, the shallow thermocline is still maintained in the southwestern Pacific and corresponds to the anomalous southward interior transport and northward western boundary at 9°S. Therefore, as the net mass transport at 9°N weakens, the net transport at 9°S becomes the dominant process of discharging. In short, the north–south asymmetry of the transport is related to the southward migration of westerly wind, when El Niño events reach their peak amplitude.

In summary, we investigate the relationship between variations in the STCs and those in the equatorial fields (SST, wind stress curl, and WWV) over the Pacific basin using the SODA reanalysis product. It is demonstrated that at interannual time scales, the interior STC transport is closely related to wind and equatorial SST as an

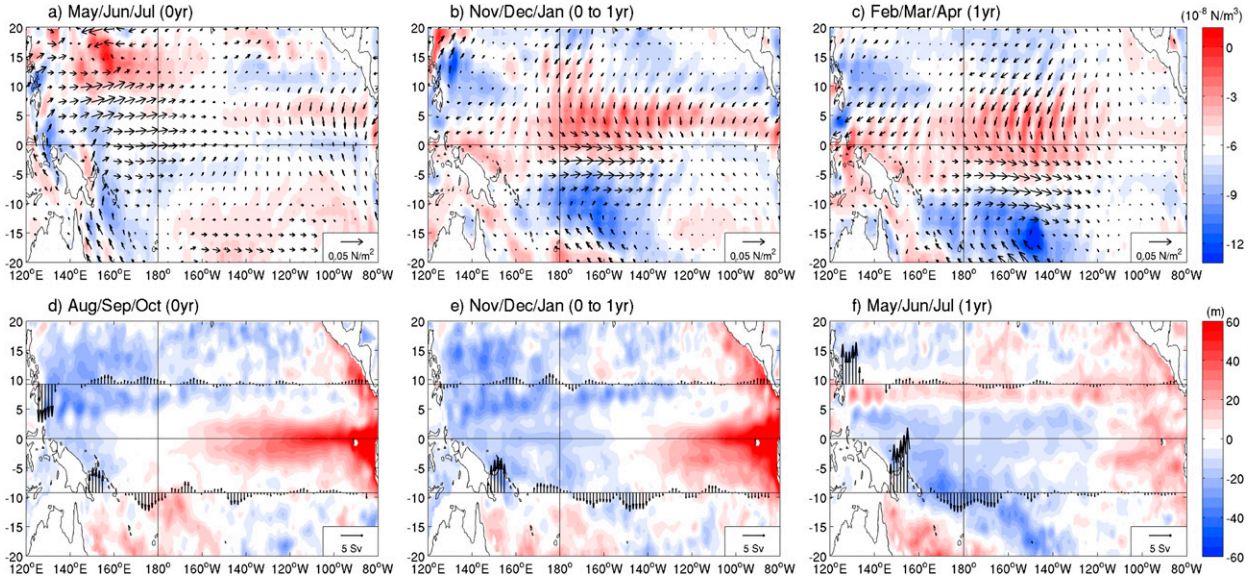

FIG. 16. Composite maps of (a)–(c) the wind stress anomaly (vectors) and the wind stress curl anomaly (shading) and (d)–(f) the depth of 26-σ_θ anomaly (shading) and meridional transport anomaly (western boundary transport and interior STC transport) zonally integrated between each 10° longitude along 9°N and 9°S (vectors) during the El Niño events in 1972/73, 1976/77, 1982/83, and 1997/98.

essential process for ENSO evolution. The correlation analysis of the indices of the interior STCs, equatorial WWV, wind stress curl, and SST anomalies reveals the dominant time intervals involved in different phases of the existing recharge–discharge mechanisms for the ENSO cycle. By analyzing the relationships between the STCs and wind and SST, we provide a possible connection of the STC variability to ENSO. As a result, our study can be valuable not only for understanding ENSO variability in the tropics, but also for interactions between the tropics and subtropics.

In addition to the conclusions stated above, the recharge–discharge processes exhibit some important features that are not fully addressed in the current study because their scopes are beyond the focus, but warrant discussions here. First, the correlation pattern of SST with the eastern interior STC transport shows that the major SST anomaly center shifts to the central Pacific (Fig. 7). This type of ENSO has been referred to as the central Pacific (CP) ENSO (Kao and Yu 2009), date line ENSO (Larkin and Harrison 2005), ENSO Modoki (Ashok et al. 2007), or warm pool ENSO (Kug et al. 2009), while the conventional ENSO is referred to as the eastern Pacific (EP) ENSO (Kao and Yu 2009). Our study indicates that the western part of interior STC transport is predominant in all ENSO events, although the eastern part of STC transport becomes appreciable during CP ENSO events. As a result, an attempt to identify EP and CP ENSO from the STC transport alone cannot be realized. The contrast between western and eastern parts of interior STC transport can only be seen when the STC transport is composited according to the two types of ENSO, like the finding by Singh and Delcroix (2013) who analyzed geostrophic transport by two types of ENSO events to show the transport in the eastern Pacific was more enhanced in CP than EP ENSO events.

Another feature to note is the decadal variation in the recharge–discharge processes. McPhaden (2012) noticed that the relationship between the equatorial SST and WWV changed in the first decade of the twenty-first century. He attributed the change to the different types of ENSO events that occurred before and after 2000. In our study, by calculating the lead time of maximum correlation between the WWV index and equatorial SST with a 5-month running mean, we identify roughly three periods, 1960–76, 1977–99, and 2000–10, with the first and last periods showing reduced WWV lead (7-month lead for 1960–76 and 4-month lead for 2000–10) over ENSO compared to the period in between (9-month lead). Bunge and Clarke (2014) also found the same relationship in similar decadal periods (pre-1973, 1974–97, and post-1998).

Finally, the mechanism linking tropical SST variability at decadal time scales with Pacific STCs is an important subject as discussed in previous studies (Klinger et al. 2002; Nonaka et al. 2002; Zhang and McPhaden 2006). We also find that the interior STC transport is largely anticorrelated with equatorial SST at decadal time scales. Furthermore, the correlation patterns between STCs, the fields of SST, and zonal wind stress at decadal time scales is similar to Pacific decadal oscillation (PDO). The results indicate that the interior STC transport is significantly correlated with tropical SST at decadal time scales, but the physical connection awaits further studies.

Acknowledgments. The authors thank all colleagues and students who contributed to this study. This work is supported by the National Science Council (NSC_101-2745-M-002-003-ASP).

REFERENCES

Alexander, M., H. Seo, S. P. Xie, and J. D. Scott, 2012: ENSO's impact on the gap wind regions of the eastern tropical Pacific Ocean. *J. Climate,* **25,** 3549–3565, doi:10.1175/JCLI-D-11-00320.1.

An, S., and I. Kang, 2000: A further investigation of the recharge oscillator paradigm for ENSO using a simple coupled model with the zonal mean and eddy separated. *J. Climate,* **13,** 1987–1993, doi:10.1175/1520-0442(2000)013<1987:AFIOTR>2.0.CO;2.

Ashok, K., S. K. Behera, S. A. Rao, H. Y. Weng, and T. Yamagata, 2007: El Niño Modoki and its possible teleconnection. *J. Geophys. Res.,* **112,** C11007, doi:10.1029/2006JC003798.

Bosc, C., and T. Delcroix, 2008: Observed equatorial Rossby waves and ENSO-related warm water volume changes in the equatorial Pacific Ocean. *J. Geophys. Res.,* **113,** C06003, doi:10.1029/2007JC004613.

Bunge, L., and A. J. Clarke, 2014: On the warm water volume and its changing relationship with ENSO. *J. Phys. Oceanogr.,* **44,** 1372–1385, doi:10.1175/JPO-D-13-062.1.

Capotondi, A., M. A. Alexander, C. Deser, and M. J. McPhaden, 2005: Anatomy and decadal evolution of the Pacific subtropical–tropical cells (STCs). *J. Climate,* **18,** 3739–3758, doi:10.1175/JCLI3496.1.

Carton, J. A., and B. S. Giese, 2008: A reanalysis of ocean climate using Simple Ocean Data Assimilation (SODA). *Mon. Wea. Rev.,* **136,** 2999–3017, doi:10.1175/2007MWR1978.1.

——, ——, and S. A. Grodsky, 2005: Sea level rise and the warming of the oceans in the Simple Ocean Data Assimilation (SODA) ocean reanalysis. *J. Geophys. Res.,* **110,** C09006, doi:10.1029/2004JC002817.

Clarke, A. J., S. Van Gorder, and G. Colantuono, 2007: Wind stress curl and ENSO discharge/recharge in the equatorial Pacific. *J. Phys. Oceanogr.,* **37,** 1077–1091, doi:10.1175/JPO3035.1.

Compo, G. P., J. S. Whitaker, and P. D. Sardeshmukh, 2006: Feasibility of a 100-year reanalysis using only surface pressure data. *Bull. Amer. Meteor. Soc.,* **87,** 175–190, doi:10.1175/BAMS-87-2-175.

——, and Coauthors, 2011: The Twentieth Century Reanalysis Project. *Quart. J. Roy. Meteor. Soc.,* **137,** 1–28, doi:10.1002/qj.776.

Giese, B. S., and S. Ray, 2011: El Niño variability in Simple Ocean Data Assimilation (SODA), 1871–2008. *J. Geophys. Res.,* **116,** C02024, doi:10.1029/2010JC006695.

Gill, A. E., 1982: *Atmosphere-Ocean Dynamics.* Academic Press, 662 pp.

Harrison, D. E., 1987: Monthly mean island surface winds in the central tropical Pacific and El Niño events. *Mon. Wea. Rev.,* **115,** 3133–3145, doi:10.1175/1520-0493(1987)115<3133:MMISWI>2.0.CO;2.

——, and N. K. Larkin, 1998: El Niño–Southern Oscillation sea surface temperature and wind anomalies, 1946–1993. *Rev. Geophys.,* **36,** 353–399, doi:10.1029/98RG00715.

——, and G. A. Vecchi, 1999: On the termination of El Niño. *Geophys. Res. Lett.,* **26,** 1593–1596, doi:10.1029/1999GL900316.

Hazeleger, W., R. Seager, M. A. Cane, and N. H. Naik, 2004: How can tropical Pacific Ocean heat transport vary? *J. Phys. Oceanogr.,* **34,** 320–333, doi:10.1175/1520-0485(2004)034<0320:HCTPOH>2.0.CO;2.

Hu, Z.-Z., A. Kumar, Y. Xue, and B. Jha, 2014: Why were some La Niñas followed by another La Niña? *Climate Dyn.,* **42,** 1029–1042, doi:10.1007/s00382-013-1917-3.

Ishida, A., Y. Kashino, S. Hosoda, and K. Ando, 2008: North-south asymmetry of warm water volume transport related with El Niño variability. *Geophys. Res. Lett.,* **35,** L18612, doi:10.1029/2008GL034858.

Jin, F. F., 1997a: An equatorial ocean recharge paradigm for ENSO. Part I: Conceptual model. *J. Atmos. Sci.,* **54,** 811–829, doi:10.1175/1520-0469(1997)054<0811:AEORPF>2.0.CO;2.

——, 1997b: An equatorial ocean recharge paradigm for ENSO. Part II: A stripped-down coupled model. *J. Atmos. Sci.,* **54,** 830–847, doi:10.1175/1520-0469(1997)054<0830:AEORPF>2.0.CO;2.

Kao, H. Y., and J. Y. Yu, 2009: Contrasting eastern Pacific and central Pacific types of ENSO. *J. Climate,* **22,** 615–632, doi:10.1175/2008JCLI2309.1.

Kessler, W. S., 2002: Is ENSO a cycle or a series of events? *Geophys. Res. Lett.,* **29,** 2125, doi:10.1029/2002GL015924.

Klinger, B. A., J. P. McCreary, and R. Kleeman, 2002: The relationship between oscillating subtropical wind stress and equatorial temperature. *J. Phys. Oceanogr.,* **32,** 1507–1521, doi:10.1175/1520-0485(2002)032<1507:TRBOSW>2.0.CO;2.

Kug, J.-S., and I.-S. Kang, 2006: Interactive feedback between ENSO and the Indian Ocean. *J. Climate,* **19,** 1784–1801, doi:10.1175/JCLI3660.1.

——, F. F. Jin, and S. I. An, 2009: Two types of El Niño events: Cold tongue El Niño and warm pool El Niño. *J. Climate,* **22,** 1499–1515, doi:10.1175/2008JCLI2624.1.

Kumar, A., and Z.-Z. Hu, 2014: Interannual variability of ocean temperature along the equatorial Pacific in conjunction with ENSO. *Climate Dyn.,* **42,** 1243–1258, doi:10.1007/s00382-013-1721-0.

Larkin, N. K., and D. E. Harrison, 2002: ENSO warm (El Niño) and cold (La Niña) event life cycles: Ocean surface anomaly patterns, their symmetries, asymmetries, and implications. *J. Climate,* **15,** 1118–1140, doi:10.1175/1520-0442(2002)015<1118:EWENOA>2.0.CO;2.

——, and ——, 2005: Global seasonal temperature and precipitation anomalies during El Niño autumn and winter. *Geophys. Res. Lett.,* **32,** L16705, doi:10.1029/2005GL022860.

Lee, T., and I. Fukumori, 2003: Interannual-to-decadal variations of tropical–subtropical exchange in the Pacific Ocean: Boundary versus interior pycnocline transports. *J. Climate,* **16,** 4022–4042, doi:10.1175/1520-0442(2003)016<4022:IVOTEI>2.0.CO;2.

Lengaigne, M., J. Boulanger, C. Meinkes, and H. Spencer, 2006: Influence of the seasonal cycle on the termination of El Niño events in a coupled general circulation model. *J. Climate,* **19,** 1850–1868, doi:10.1175/JCLI3706.1.

Lu, P., J. P. McCreary Jr., and B. A. Klinger, 1998: Meridional circulation cells and the source waters of the Pacific Equatorial Undercurrent. *J. Phys. Oceanogr.,* **28,** 62–84, doi:10.1175/1520-0485(1998)028<0062:MCCATS>2.0.CO;2.

McCreary, J. P., Jr., and P. Lu, 1994: Interaction between the subtropical and equatorial ocean circulations: The subtropical cell. *J. Phys. Oceanogr.,* **24,** 466–497, doi:10.1175/1520-0485(1994)024<0466:IBTSAE>2.0.CO;2.

McGregor, S., A. Timmermann, N. Schneider, M. F. Stuecker, and M. H. England, 2012: The effect of the South Pacific convergence zone on the termination of El Niño events and the meridional asymmetry of ENSO. *J. Climate,* **25,** 5566–5586, doi:10.1175/JCLI-D-11-00332.1.

McPhaden, M. J., 2012: A 21st century shift in the relationship between ENSO SST and warm water volume anomalies. *Geophys. Res. Lett.,* **39,** L09706, doi:10.1029/2012GL051826.

——, and D. X. Zhang, 2002: Slowdown of the meridional overturning circulation in the upper Pacific Ocean. *Nature,* **415,** 603–608, doi:10.1038/415603a.

Meinen, C. S., and M. J. McPhaden, 2000: Observations of warm water volume changes in the equatorial Pacific and their relationship to El Niño and La Niña. *J. Climate,* **13,** 3551–3559, doi:10.1175/1520-0442(2000)013<3551:OOWWVC>2.0.CO;2.

——, and ——, 2001: Interannual variability in warm water volume transports in the equatorial Pacific during 1993–99. *J. Phys. Oceanogr.,* **31,** 1324–1345, doi:10.1175/1520-0485(2001)031<1324:IVIWWV>2.0.CO;2.

Nagura, M., K. Ando, and K. Mizuno, 2008: Pausing of the ENSO cycle: A case study from 1998 to 2002. *J. Climate,* **21,** 342–363, doi:10.1175/2007JCLI1765.1.

Nonaka, M., S.-P. Xie, and J. P. McCreary, 2002: Decadal variations in the subtropical cells and equatorial Pacific SST. *Geophys. Res. Lett.,* **29,** doi:10.1029/2001GL013717.

Ohba, M., and H. Ueda, 2009: Role of nonlinear atmospheric response to SST on the asymmetric transition process of ENSO. *J. Climate,* **22,** 177–192, doi:10.1175/2008JCLI2334.1.

——, and M. Watanabe, 2012: Role of the Indo-Pacific interbasin coupling in predicting asymmetric ENSO transition and duration. *J. Climate,* **25,** 3321–3335, doi:10.1175/JCLI-D-11-00409.1.

Okumura, Y. M., and C. Deser, 2010: Asymmetry in the duration of El Niño and La Niña. *J. Climate,* **23,** 5826–5843, doi:10.1175/2010JCLI3592.1.

——, M. Ohba, C. Deser, and H. Ueda, 2011: A proposed mechanism for the asymmetric duration of El Niño and La Niña. *J. Climate,* **24,** 3822–3829, doi:10.1175/2011JCLI3999.1.

Rayner, N. A., D. E. Parker, E. B. Horton, C. K. Folland, L. V. Alexander, D. P. Rowell, E. C. Kent, and A. Kaplan, 2003: Global analyses of sea surface temperature, sea ice, and night marine air temperature since the late nineteenth century. *J. Geophys. Res.,* **108,** 4407, doi:10.1029/2002JD002670.

Rothstein, L. M., R.-H. Zhang, A. J. Busalacchi, and D. Chen, 1998: A numerical simulation of the mean water pathways in the subtropical and tropical Pacific Ocean. *J. Phys. Oceanogr.,* **28,** 322–343, doi:10.1175/1520-0485(1998)028<0322:ANSOTM>2.0.CO;2.

Singh, A., and T. Delcroix, 2013: Eastern and central Pacific ENSO and their relationships to the recharge/discharge oscillator paradigm. *Deep-Sea Res. I,* **82,** 32–43, doi:10.1016/j.dsr.2013.08.002.

Springer, S. R., M. J. McPhaden, and A. J. Busalacchi, 1990: Oceanic heat content variability in the tropical Pacific during the 1982–1983 El Niño. *J. Geophys. Res.,* **95,** 22 089–22 101, doi:10.1029/JC095iC12p22089.

Stuecker, M. F., A. Timmermann, F.-F. Jin, S. McGregor, and H.-L. Ren, 2013: A combination mode of the annual cycle and the El Niño/Southern Oscillation. *Nat. Geosci.,* **6,** 540–544, doi:10.1038/ngeo1826.

Vecchi, G., and D. E. Harrison, 2003: On the termination of the 2002–03 El Niño event. *Geophys. Res. Lett.,* **30,** 1964, doi:10.1029/2003GL017564.

Wang, X., F.-F. Jin, and Y. Wang, 2003: A tropical ocean recharge mechanism for climate variability. Part I: Equatorial heat content changes induced by the off-equatorial wind. *J. Climate,* **16,** 3585–3598, doi:10.1175/1520-0442(2003)016<3585:ATORMF>2.0.CO;2.

Whitaker, J. S., G. P. Compo, X. Wei, and T. M. Hamill, 2004: Reanalysis without radiosondes using ensemble data assimilation. *Mon. Wea. Rev.,* **132,** 1190–1200, doi:10.1175/1520-0493(2004)132<1190:RWRUED>2.0.CO;2.

White, W. B., G. A. Meyers, J. R. Donguy, and S. E. Pazan, 1985: Short-term climate variability in the thermal structure of the Pacific Ocean during 1979–82. *J. Phys. Oceanogr.,* **15,** 917–935, doi:10.1175/1520-0485(1985)015<0917:STCVIT>2.0.CO;2.

Wyrtki, K., 1975: El Niño—The dynamic response of the equatorial Pacific Ocean to atmospheric forcing. *J. Phys. Oceanogr.,* **5,** 572–584, doi:10.1175/1520-0485(1975)005<0572:ENTDRO>2.0.CO;2.

——, 1985: Water displacements in the Pacific and the genesis of El Niño cycles. *J. Geophys. Res.,* **90,** 7129–7132, doi:10.1029/JC090iC04p07129.

Zhang, D. X., and M. J. McPhaden, 2006: Decadal variability of the shallow Pacific meridional overturning circulation: Relation to tropical sea surface temperatures in observations and climate change models. *Ocean Modell.,* **15,** 250–273, doi:10.1016/j.ocemod.2005.12.005.